www.czasopisma.pan.pl PAN www.journals.pan.pl
Chemical and Process Engineering 2020, 41 (3), 197–208
DOI: 10.24425/cpe.2020.132542

Influence of humidity on carbon dioxide adsorption on zeolite 13X

Kamila Zabielska, Tomasz Aleksandrzak, Elżbieta Gabruś*

Faculty of Chemical Technology and Engineering, West Pomeranian University of Technology, Szczecin, al. Piastów 42, 71-065 Szczecin, Poland

Greenhouse gases such as carbon dioxide and water vapour can be captured from gas streams on a zeolite 13X adsorbent. Experimental water vapour adsorption isotherms and kinetic curves were measured in the temperature range of 293–393 K and pressure up to 2100 Pa. The equilibrium data were developed with Toth and Sips multi-temperature isotherm models. The results of the process rate studies were described using pseudo-first and pseudo-second order kinetic models. Findings were compared with our own results of CO_2 adsorption studies on the same zeolite.

Keywords: carbon dioxide, water vapour, zeolite 13X, adsorption equilibrium

1. INTRODUCTION

Global warming is a problem of the beginning of 21^{st} century. Carbon dioxide (CO_2) is the main greenhouse gas emitted by human activity mainly in combustion of fossil fuels (Ben-Mansour et al., 2016). One of the perspective methods for reducing emission of CO_2 to atmosphere are adsorption-based separation processes such as pressure, temperature, and vacuum swing adsorption (Hefti and Mazzotti, 2018; Li et al., 2014; Marx et al., 2013). In these processes a flue gas is passed through a fixed bed filled with an adsorbent. The most popular adsorbent for CO_2 capturing is zeolite 13X (Hefti and Mazzotti, 2018). The industrial flue gas mainly consists of nitrogen, water, carbon dioxide and oxygen. During the process, CO_2 is captured by the adsorbent in presence of water vapour, because the amount of water in the flue gas is 3–10% (Li et al., 2014). Water has high dipole moment, and this caused strong bond with surface of zeolite (Marx et al., 2013), but the amount and rate of its adsorption requires further research.

The basis for the design of adsorption installations is knowledge of the equilibrium and kinetics of the adsorption process over a wide temperature range (Brandani and Ruthven, 2004; Kim et al., 2003; Wang and LeVan, 2009). In most papers relating to adsorption of water vapour on zeolite 13X only adsorption equilibrium is tested. Moreover, results are different depending on the manufacturer of the zeolite (Brandani and Ruthven, 2004; Hefti and Mazzotti, 2018; Kim et al., 2003; Li et al., 2008; 2009; Rege et al., 2000; Sayılgan et al., 2016; Son et al., 2019; Wang and LeVan, 2009; Wynnyk et al., 2018). The adsorption kinetics is neglected, which is a mistake due to the short residence time of individual stages in cyclic adsorption processes. Only in two papers measurements of kinetics for zeolite 13X – water vapour system were presented. Ryu et al. (2001) conducted measurement at 298 and 398 K while Sayılgan et al. (2016) measured the adsorption kinetics at 393 K.

* Corresponding author, e-mail: Elzbieta.Gabrus@zut.edu.pl

In this paper the adsorption equilibrium and kinetics for zeolite 13X – water vapour system at a wide range of temperature were examined. The experimental data obtained were correlated with chosen models. Obtained experimental data of equilibrium and kinetics were compared with measurement of zeolite 13X–CO_2.

2. MATERIALS AND METHODS

2.1. Characteristics of adsorbent

Experimental research concerned adsorption equilibrium of water vapour onto zeolite 13X, which was manufactured by Hurtgral (Poland). Basic physical properties of the adsorbent are presented in Table 1.

Table 1. Physical properties of zeolite 13X

Property	Value
Shape	Beads
Nominal pore diameter, Å	10
Particle diameter, mm	1.7–2.5
Bulk density, kg/m^3	700

2.2. Experimental apparatus and measurement methodology

Studies of adsorption equilibrium and kinetics of water vapour on zeolite 13X were performed using a static gravimetric analyser (IGA-002, Hiden Isochema, United Kingdom). The central element of the IGA system is a balance with weighing resolution of 0.1 μg. The sample was situated in a sieve made of stainless steel, which was hung to the balance using a gold chain. The adsorbent weight was about 78 mg. The sample was placed in a metal reactor, wherein an ultra-high vacuum was possible. The reactor was thermostated using a circulation water bath GR 150 (Grant Instruments, United Kingdom) or heated with electric furnace Cryofurnace (Hiden Isochema, United Kingdom). The sample temperature was measured using a Pt 100 sensor and regulated by the PID controller with the accuracy of ±0.05 K for the water bath and ±0.1 K for the furnace. The pressure inside the reactor was measured using a pressure gauge with a sensitivity of ±0.625 Pa. Before each examination, the sample was degassed "*in situ*" for 2 hours at the temperature of 423 K and vacuum of 10^{-6} Pa. After degassing, the adsorption kinetics and equilibrium were measured for given temperature and pressure values (Zabielska et al., 2018).

2.3. Adsorption equilibrium

Determination of adsorption equilibrium is a key step for performing process design and optimization. Adsorption equilibrium in the gas-solid system is represented by:

- adsorption isobar (p = const)

$$q = f(T)_p \tag{1}$$

- adsorption isotherm (t = const)

$$q = f(p)_T \tag{2}$$

The equilibrium adsorption process can be described by the isotherm equation, which can be represented using 6 different types according to the International Union of Pure and Applied Chemistry classification (IUPAC). Thermodynamic equilibrium data allows to describe texture of adsorbents and to adjust basic parameters of the process in selected adsorption system. The adsorption isotherm also provides information about the thermal effect of the process. During adsorption of water vapour in the high relative partial pressure of adsorbate, capillary condensation often occurs (Do, 1998; Keller and Staudt, 2005; Thomas and Crittenden, 1998).

2.4. Adsorption isotherm models

In the work, isotherm models were fitted to the measured adsorption equilibrium points at various temperatures to increase the usefulness of the experimental data. The multi-temperature models of Sips and Toth adsorption isotherms were used. These equations are useful in pressure swing adsorption (PSA) simulation due to their simple mathematical form.

2.4.1. Sips model

Considering the problem of continuous increase of adsorbed amount with increasing pressure in the Freundlich model, Sips presented an equation that has a similar form to the Freundlich equation, but has a finite limit when the pressure is high (Thomas and Crittenden, 1998).

$$q = q_m(T)\frac{b(T)\cdot p^{n(T)}}{1 + b(T)\cdot p^{n(T)}} \tag{3}$$

In this form Eq. (3) resembles the Langmuir equation. The difference is an additional parameter n characterizing the system heterogeneity. In Eq. (3) q_m, b and n are characteristic coefficients dependent on temperature T according to the relations:

$$q_m(T) = a_{0LF} + \frac{a_{1LF}}{T} + \frac{a_{2LF}}{T^2} \tag{4}$$

$$b(T) = \exp\left(b_{0LF} + \frac{b_{1LF}}{T} + \frac{b_{2LF}}{T^2}\right) \tag{5}$$

$$n(T) = n_{0LF} + \frac{n_{1LF}}{T} \tag{6}$$

After substituting Eqs. (4)–(6) into Eq. (3) the mathematical form of multitemperature Sips adsorption isotherm is obtained (Ayawei et al., 2017; Do, 1998; Keller and Staudt, 2005):

$$q = a_{0LF} + \frac{a_{1LF}}{T} + \frac{a_{2LF}}{T^2}\frac{\exp\left(b_{0LF} + \frac{b_{1LF}}{T} + \frac{b_{2LF}}{T^2}\right)\cdot p^{n_{0LF}+\frac{n_{1LF}}{T}}}{1 + \exp\left(b_{0LF} + \frac{b_{1LF}}{T} + \frac{b_{2LF}}{T^2}\right)\cdot p^{n_{0LF}+\frac{n_{1LF}}{T}}} \tag{7}$$

2.4.2. Toth model

The Toth isotherm is a semi-empirical modification of the Langmuir equation to reduce the error between experimental and calculated equilibrium data. The Toth equation describes adsorption in a monolayer. This model is related with surface diversity and interactions of adsorbed particles. The relation of the Toth model can be represented as (Do, 1998; Keller and Staudt, 2005):

$$q = q_m\frac{p}{(b(T) + p^{n_T})^{1/n_T}} \tag{8}$$

In Eq. (8) the coefficient b depends on the temperature according to the relation:

$$b(T) = b_{0T} \cdot \exp\left(-\frac{n_T \cdot \Delta H}{R \cdot T}\right) \tag{9}$$

The mathematical form of multitemperature Toth adsorption isotherm is:

$$q = q_m \frac{p}{\left(b_{0T} \cdot \exp\left(-\frac{n_T \cdot \Delta H}{R \cdot T}\right) + p^{n_T}\right)^{1/n_T}} \tag{10}$$

In addition to the above-mentioned models, adsorption equilibrium can also be described by other isotherms such as the Brunauer–Emmett–Teller (BET), Dubinin–Radushkevich, Temkin models (Ayawei et al., 2017; Thomas and Crittenden, 1998). These models were not used in the research due to their insufficient matching with experimental data.

Depending on the linear expression of each isotherm and kinetic curve, all the models parameters could be acquired by linear regression. The chosen equilibrium and kinetics equations were fitted to the experimental data using Statistica 13.1 software (Statsoft).

In this study, the best fitting quality was found based on four different error functions, which were calculated based on the following Eqs. (11)–(13):

a) Average relative error (*ARE*):

$$ARE = \frac{1}{n}\sum_{i=1}^{n}\left|\frac{q_{\text{exp}} - q_{\text{sim}}}{q_{\text{exp}}}\right| \tag{11}$$

b) Root mean sum-of-squares error (*RMSE*):

$$RMSE = \sqrt{\frac{1}{n}\sum_{i=1}^{n}(q_{\text{exp}} - q_{\text{sim}})^2} \tag{12}$$

c) Chi-squared statistic (χ^2):

$$\chi^2 = \sum_{i=1}^{n}\frac{(q_{\text{exp}} - q_{\text{sim}})^2}{q_{\text{sim}}} \tag{13}$$

In addition to these formulas, the coefficients of determination R^2 were calculated for each isotherm and kinetic model (Ayawei et al., 2017; Tan and Hameed, 2017).

2.5. Adsorption kinetics

The kinetics of the adsorption process can be described by knowing the solid structure and phase equilibrium. The mechanism of this process consists of three stages. The first is the penetration of the substance adsorbed from the fluid phase core into the outer surface of the adsorbent (external diffusion). The second is the diffusion of the adsorbate in the adsorbent pores (internal diffusion). The last step is the adsorption of the adsorbed component on the outer and inner surface of the pores called the actual act of adsorption (Rashidi et al., 2013; Qiu et al., 2009).

The rate of the adsorption process is the increase in the amount of substance adsorbed in time $q_t = f(t)$. Kinetic coefficients are determined based on the results of adsorption kinetics measurements on single grains or on thin layers of adsorbent. Internal diffusion describes the effective diffusion coefficient. External diffusion describes the mass transfer coefficient. The kinetic properties characterizing the adsorption rate inform about the mechanisms of the process in a given system and depend on: initial concentration, contact

time and adsorbent mass. Kinetic models are very helpful in recognizing mechanisms (Petrus et al., 2006; Thomas and Crittenden, 1998).

To correlate models with kinetic experimental data pseudo-first order and pseudo-second order reaction models were selected.

2.5.1. Pseudo-first order (PFO) equation

In 1898, Lagergren presented a pseudo-first order equation to describe the kinetics of the adsorption process. This equation is considered the initial model, which refers to the adsorption rate based on the adsorption capacity and can be represented in a linear form (Petrus et al., 2006):

$$\ln\left(\frac{q_{e1}}{q_{e1}-q_{t1}}\right) = k_1 t \tag{14}$$

Equation (14) can be transformed so that it is possible to calculate the concentration of the adsorbed substance in the solid grain after a specified time t (Petrus et al., 2006; Qiu et al., 2009):

$$q_{t1} = q_{e1}\left(1 - e^{-k_1 t}\right) \tag{15}$$

The values of pseudo-first-order kinetic parameter k_1 and q_{e1} are determined from the slope and intercept of the plots of $\ln(q_{e1} - q_{t1})$ versus t. If the model is applicable, the relationship should be linear.

2.5.2. Pseudo-second order (PSO) equation

In 1995, Ho described a pseudo-second order kinetics, which can be represented by a linear equation (Petrus et al., 2006; Qiu et al., 2009):

$$\frac{1}{q_{t2}} = \frac{1}{k_2 q_{e2}^2} + \frac{t}{q_{e2}} \tag{16}$$

$$r_2 = k_2 q_{e2}^2 \tag{17}$$

Eq. (16) can be transformed into a form describing the change in adsorbate concentration in the sorbent in a specified time t (Petrus et al., 2006; Qiu et al., 2009; Rashidi et al., 2013):

$$q_{t2} = \frac{q_{e2}^2 k_2 t}{1 + k_2 q_{e2} t} \tag{18}$$

The pseudo second-order kinetic constant k_2 and the theoretical equilibrium adsorption q_{e2} can be obtained from the slope and intercept of the plots of t/q_{t2} versus t. If the model is suitable, the relationship should be linear.

3. RESULTS

Figure 1 shows a comparison of adsorption isotherms of water vapour (Fig. 1a) and carbon dioxide (Fig. 1b) on zeolite 13X between our own experimental data with data found in other papers for the temperature of 293 K. The highest adsorption value for water vapour was obtained by Kim et al. (2016) and it is 18.86 mol/kg under pressure of 2200 Pa. For carbon dioxide the highest adsorption value was obtained by Ling et al. (2014) and it is 4.34 mol/kg under pressure of 102 300 Pa.

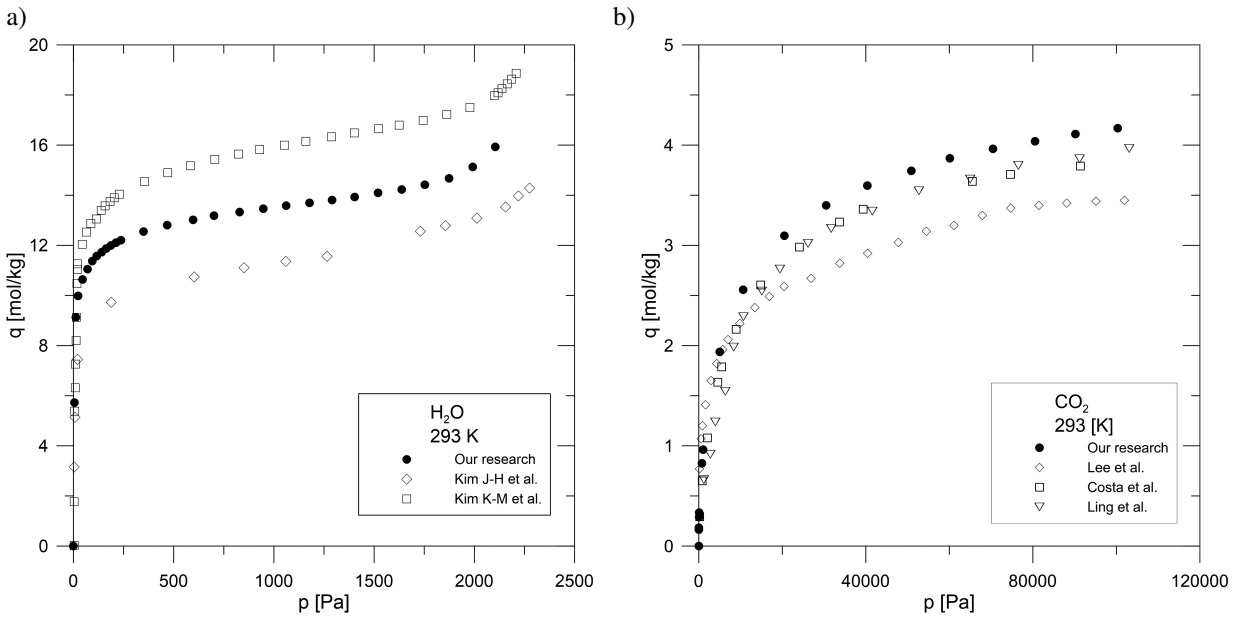

Fig. 1. Comparison of experimental isotherms for water vapour adsorption with other researchers onto zeolite 13X at 293 K (a) and for carbon dioxide (b)

The graphs (Figs. 1a and 1b) show that the use of the same type of adsorbent, but different manufacturers requires experimental determination of adsorption equilibrium every time (Costa et al., 1991; Kim et al., 2003; 2016; Lee et al., 2002; Ling et al., 2014; Zabielska et al., 2018).

As a result of measurements, the adsorption isotherms for water vapour–zeolite 13X system were determined at temperatures: 293 K to 393 K and under pressures up to 2100 Pa (Fig. 3).

The shape of isotherms for the water vapour-zeolite 13X system for different temperatures indicates that we are dealing with isotherms of type II according to the IUPAC classification (Fig. 2). This type describes adsorption on macroporous adsorbents showing strong and weak adsorbate-adsorbent interactions. Adsorption capacity increases in proportion to the pressure, this increase is decreasing, then reaches a constant value and slowly increases due to capillary condensation.

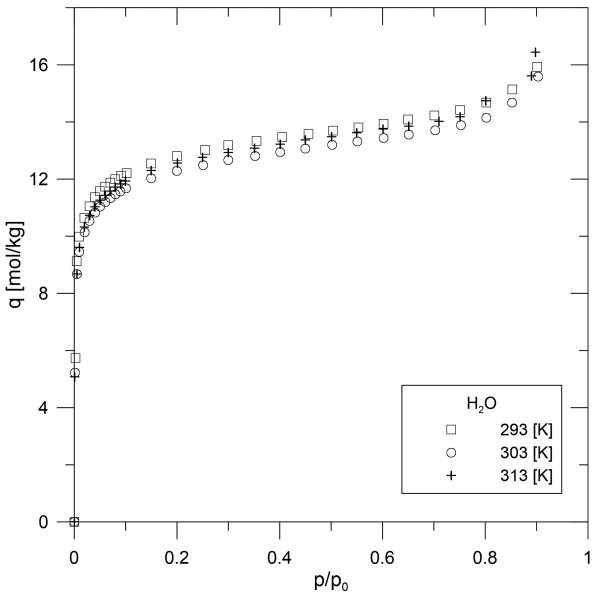

Fig. 2. Experimental isotherms for water vapour adsorption onto zeolite 13X at various temperatures

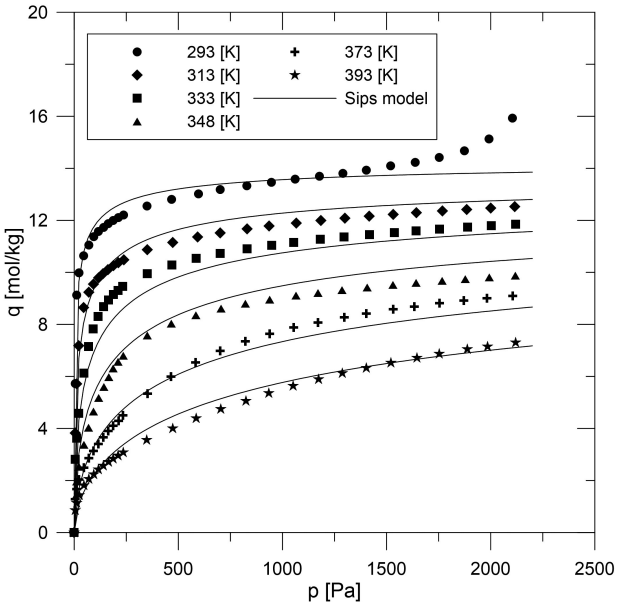

Fig. 3. Experimental and correlated (Sips equation) isotherms for water vapour adsorption onto zeolite 13X at various temperatures

The experimental and correlated by the Sips model isotherms for water vapour-zeolite 13X system at various temperatures and under pressures up to 2100 Pa are presented in Fig. 3.

The highest adsorption capacity of 15.93 mol/kg was obtained at a temperature of 293 K and a pressure of 2104 Pa. During the temperature increase the adsorption capacity was decreased, and at 393 K it was 7.31 mol/kg for 2120 kPa. The multitemperature adsorption isotherm models of Sips and Toth were fitted to the experimental data. The obtained values of isotherm parameters for all the equilibrium models and error functions are presented in Table 2.

Table 2. Multitemperature adsorption isotherm parameters and error functions for Sips and Toth model for the water vapour-zeolite 13X

Isotherm model parameter	Parameter value	*ARE* %	*RMSE* –	χ^2 –	R^2 –
Sips					
a_{0S}, mol/kg	5.9812				
a_{1S}, mol·K/kg	2476.662				
a_{2S}, mol·K^2/kg	16.3604				
b_{0S}, Pa^{-n}	–13.562	6.08	0.466	5.633	0.9870
b_{1S}, Pa^{-n}·K	3690.997				
b_{2S}, Pa^{-n}·K	20.609				
n_{0S}, –	0.728				
n_{1S}, –	–55.803				
Toth					
q_m, mol/kg	15.487				
b_{0T}, Pa^{-n}	3432.389	6.41	0.467	6.950	0.9857
n_T, –	0.366				
ΔH, J/mol	57209.177				

The best fit to the experimental data for water vapour on zeolite 13X was obtained using the Sips model with the following error demonstration: *ARE* = 6.08%, *RMSE* = 0.466, χ^2 = 5.633 and R^2 = 0.9870. Toth model also demonstrates good fit for water vapour – zeolite 13X system.

Kinetic curves for water vapour were determined for temperatures 293, 313, and 348 K and under pressure 1000 Pa and in the time range from 0 to 2000 s. These curves are compared with kinetic curves for carbon dioxide, which were carried out for temperatures: 293, 313 and 348 K and at a pressure of 5400 Pa in the time range from 0 to 1000 s.

The results of fitting the pseudo-first order and pseudo-second order models to experimental data for the kinetics of water vapour and carbon dioxide adsorption on zeolite 13X are shown in Figs. 4 and 5.

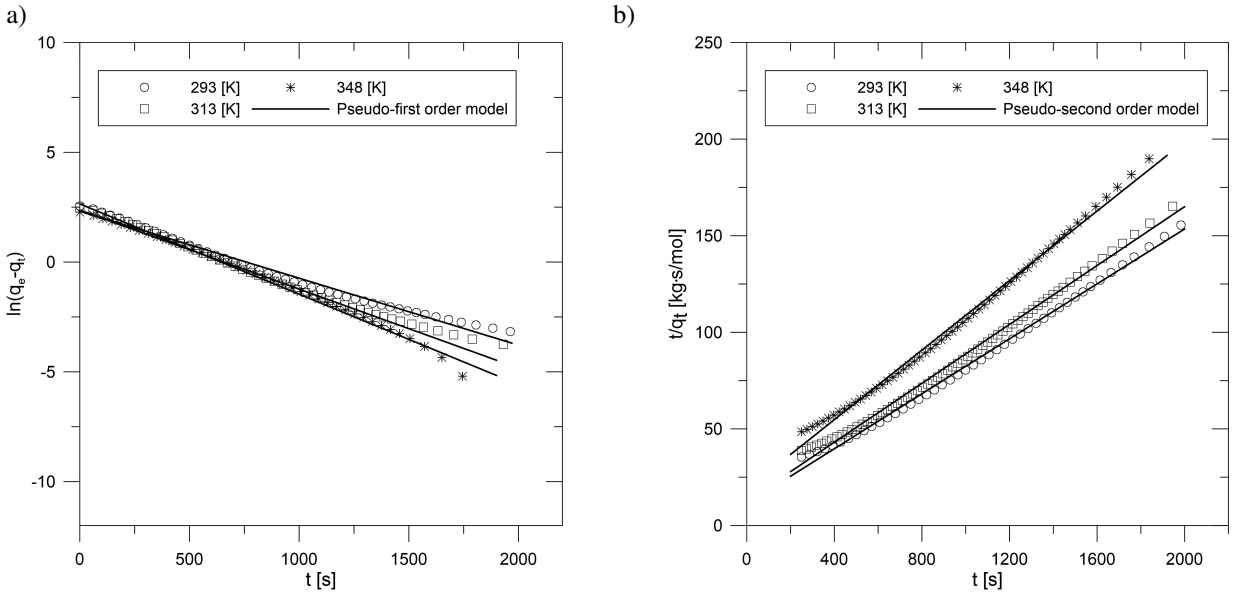

Fig. 4. Experimental and correlated (pseudo-first order model (a), pseudo-second order model (b)) kinetic curves for water vapour adsorption onto zeolite 13X at various temperatures

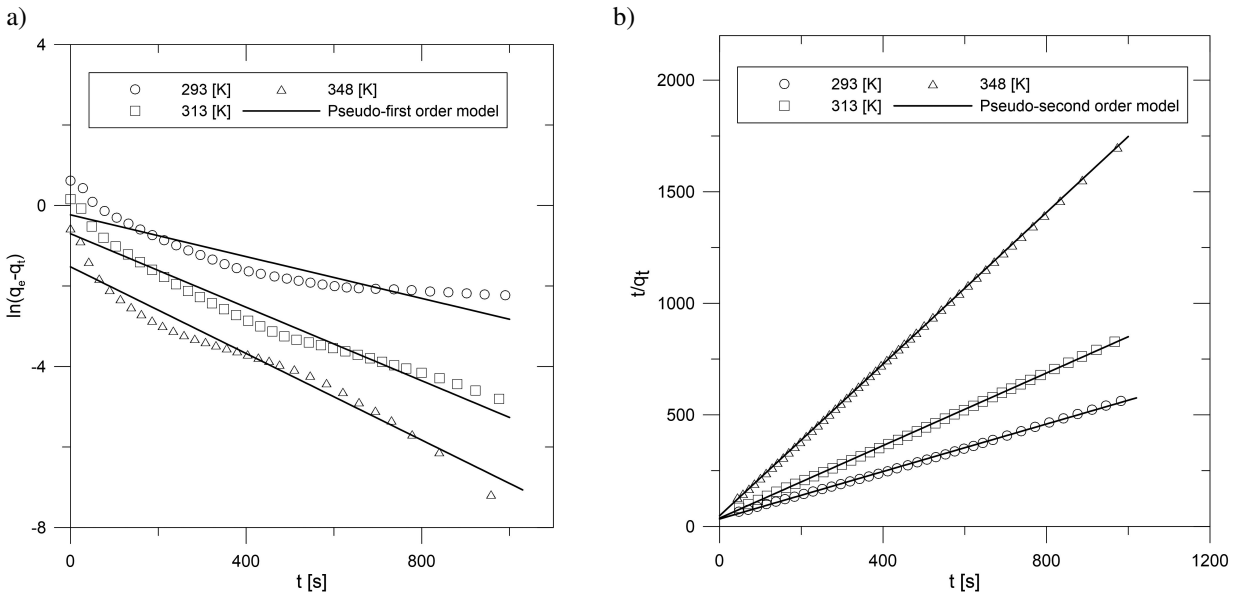

Fig. 5. Experimental and correlated (pseudo-first order model (a), pseudo-second order model (b)) kinetic curves for carbon dioxide adsorption onto zeolite 13X at various temperatures

The obtained values of constants for selected pseudo-first order, and pseudo-second order models for water vapour and carbon dioxide on zeolite 13X and error functions for individual temperatures are presented in Tables 3 and 4.

Table 3. Kinetic parameters for pseudo-first order model and error functions for water vapour and carbon dioxide on zeolite 13X

Parameter	Temperature, K					
	293	313	348	293	313	348
	Water vapour			Carbon dioxide		
q_{e1}, mol/kg	12.796	11.793	9.682	1.8535	1.17537	0.573246
$k_1 \cdot 10^3$, 1/s	3.05	3.505	4.113	2.595	4.565	5.38
ARE, %	2.31	5.30	11.15	28.31	16.22	19.06
RMSE, –	0.352	0.276	0.5423	0.432	0.183	0.111
χ^2, –	43.43	70.46	190.74	496.4	129.28	82.89
R^2, –	0.9849	0.9915	0.9820	0.8390	0.9539	0.9567

Table 4. Kinetic parameters for pseudo-second order model and error functions for water vapour and carbon dioxide on zeolite 13X

Parameter	Temperature, K					
	293	313	348	293	313	348
	Water vapour			Carbon dioxide		
q_{e2}, mol/kg	14.065	13.123	11.111	1.879	1.2299	0.588
$k_2 \cdot 10^4$, kg/(mol·s)	6.78	4.594	4.411	84.66	177.5	601.53
r_2, mol^2/(kg^2·s)	1.385	0.086	0.049	298.904	268.496	207.975
ARE, %	6.42	2.86	2.94	1.76	1.16	0.46
RMSE, –	0.869	0.378	0.287	0.029	0.015	0.003
χ^2, –	211.62	44.35	29.681	1.14	0.451	0.027
R^2,–	0.9967	0.9956	0.9953	0.9993	0.9997	1

As can be seen from Tables 3, 4 and in Figs. 4, 5, the pseudo-first order model does not reflect CO_2 kinetics, and for water vapour the temperature effects on the kinetics (fitting errors increase significantly). Therefore, the comparison of adsorption rates was made based on the pseudo-second order model, which well approximates the kinetics for both adsorption systems. The values of the kinetic coefficients for CO_2 are from 12 (293 K) to 136 (348 K) times higher than those for water.

Adsorption capacity of the zeolite 13X was found to be about five times higher for H_2O (15.3 mol/kg = 0.275 kg/kg) than that for CO_2 (1.24 mol/kg = 0.055 kg/kg) for a pressure of 2000 Pa. These two opposing aspects of CO_2 and H_2O adsorption on zeolite do not allow to apply predictive adsorptive separation but require further research in a two-component system.

4. CONCLUSIONS

The adsorption equilibrium measurements for H_2O – zeolite 13X were conducted in a wide temperature range (293 K to 393 K) and under pressures up to 2100 Pa. The highest adsorption capacity was at a temperature of 293 K and it was 15.93 mol/kg. The best fit to the equilibrium experimental data was obtained using the Sips model. Experimental data for H_2O – zeolite 13X system were compared with our previous measurements of CO_2 – zeolite 13X system. The adsorbed mass of H_2O was 5 times higher (15.3 mol/kg = 0.275 kg/kg) than that for CO_2 (1.24 mol/kg = 0.055 kg/kg). It seems that zeolite 13X adsorbed H_2O much better than CO_2, although in a column process the residence time was limited and the process kinetics played a key role. Based on the experimental research of individual equilibrium components and on literature reports (Hefti et al., 2014; Purdue and Qiao, 2018) it can be concluded that zeolite 13X reveals high affinity to water vapour, which may result in a reduction in the efficiency of removing carbon dioxide from flue gas.

The kinetic measurements were determined at temperatures: 293, 313, 348 K and under the pressure of 1000 Pa. The time needed to achieve equilibrium was about 2000 s. Pseudo-first order and pseudo-second order reaction models were correlated with experimental data. Kinetic coefficients for H_2O – zeolite 13X system are compared with our previous study for CO_2 – zeolite 13X system for the pseudo-second order model. The kinetic coefficients for CO_2 are from 12 (293 K) to 136 (348 K) times higher than that for water, which indicates that CO_2 can be adsorbed much faster than water vapour and is a competition in access to the 13X zeolite adsorption surface.

An important issue of the gas mixture adsorption is to determine the real interaction between the gas components and the adsorbent. Future two-component studies are necessary for deeper analysis. The problem of humidity influence on carbon dioxide adsorption on zeolite 13X can be solved, in practice, by using an additional desiccant layer in which moisture contained in the flue gas will be removed.

The experimental and simulation results of equilibrium and kinetics are the baseline studies for future research of cyclic adsorption processes such as Pressure, Temperature, and Vacuum Swing Adsorption.

SYMBOLS

a_{0S}	Sips isotherm parameter, mol/kg
a_{1S}	Sips isotherm parameter, mol/(kg· Pa)
a_{2S}	Sips isotherm parameter, mol· K^2/kg
ARE	average relative error, %
b_{0S}	Sips isotherm parameter, Pa^{-n}
b_{0T}	Toth isotherm parameter, Pa^{-n}
b_{1S}	Sips isotherm parameter, Pa^{-n}· K
b_{2S}	Sips isotherm parameter, Pa^{-n}· K
k_1	rate constant for pseudo first-order kinetics, 1/s
k_2	rate constant for pseudo second-order kinetics, kg/(mol·s)
n	number of experimental points
n_T	Toth isotherm parameter, –
n_{0S}	Sips isotherm parameter, –
n_{1S}	Sips isotherm parameter, –
r_2	initial adsorption rate, mol^2/kg^2·s
RMSE	root mean sum-of-squares error, –
q	adsorption capacity, mol/kg

q_{e1}	theoretical equilibrium adsorption in PFO model, mol/kg
q_{e2}	theoretical equilibrium adsorption in PSO model, mol/kg
q_{exp}	experimental adsorption capacity, mol/kg
q_m	Toth isotherm parameter, mol/kg
q_{sim}	calculated adsorption capacity, mol/kg
q_{t1}	amount of adsorption at time in pseudo-first order model, mol/kg
q_{t2}	amount of adsorption at time in pseudo-second order model, mol/kg
R	universal gas constant, J/(mol· K)
R^2	coefficient of determination
P	partial pressure of the adsorbate, Pa
t	time interval, s
T	temperature, K

Greek symbols

ΔH	heat of adsorption, J/mol
χ^2	chi-squared statistics

REFERENCES

Ayawei N., Ebelegi A.N., Wankasi D., 2017. Modelling and interpretation of adsorption isotherms. *Hindawi J. Chem.*, 3039817. DOI: 10.1155/2017/3039817.

Ben-Mansour R., Habib M.A., Bamidele O.E., Basha M., Qasem N.A.A., Peedikakkal A., Laoui T., Ali M., 2016. Carbon capture by physical adsorption: Materials, experimental investigations and numerical modeling and simulations – A review. *Appl. Energy*, 161, 225–255. DOI: 10.1016/j.apenergy.2015.10.011.

Brandani F., Ruthven D.M., 2004. The effect of water on the adsorption of CO_2 and C_3H_8 on type X zeolites. *Ind. Eng. Chem. Res.*, 43, 8339–8344. DOI: 10.1021/ie040183o.

Costa E., Calleja G., Jimenez A., Pau J., 1991. Adsorption equilibrium of ethylene, propane, propylene, carbon dioxide, and their mixtures on 13X zeolite. *J. Chem. Eng. Data*, 36, 218–224. DOI: 10.1021/je00002a020.

Do D.D., 1998. *Adsorption analysis: Equilibria and kinetics*. Imperial College Press.

Hefti M., Marx D., Joss L., Mazzotti M., 2014. Model-based process design of adsorption processes for CO_2 capture in the presence of moisture. *Energy Procedia*, 63, 2152–2159. DOI: 10.1016/j.egypro.2014.11.234.

Hefti M., Mazzotti M., 2018. Postcombustion CO_2 capture from wet flue gas by temperature swing adsorption. *Ind. Eng. Chem. Res.*, 57, 15542–15555. DOI: 0.1021/acs.iecr.8b03580.

Keller J., Staudt R., 2005. *Gas adsorption equilibria: Experimental methods and adsorption isotherms*. Springer.

Kim J.H., Lee C.H., Kim W.S., Lee J.S., Kim J.T., Suh J.K., Lee J.M., 2003. Adsorption equilibria of water vapor on alumina, zeolite 13X, and a zeolite X/activated carbon composite. *J. Chem. Eng. Data*, 48, 137–141. DOI: 10.1021/je0201267.

Kim K.-M., Oh H.-T., Lim S.-J., Ho K., Park Y., Lee C.-H., 2016. Adsorption equilibria of water vapor on zeolite 3A, Zeolite 13X, and dealuminated Y zeolite. *J. Chem. Eng. Data*, 61, 1547–15554. DOI: 10.1021/acs.jced.5b00927.

Lee J.-S., Kim J.-H., Kim J.-T., Suh J.-K., Lee J.-M., Lee C.-H., 2002. Adsorption equilibria of CO_2 on zeolite 13X and zeolite X/activated carbon composite. *J. Chem. Eng. Data*, 47, 1237–1242. DOI: 10.1021/je020050e.

Li G., Xiao P, Webley P.A., Zhang J., Singh R., Marshall M., 2008. Capture of CO_2 from high humidity flue gas by vacuum swing adsorption with zeolite 13X. *Adsorption*, 14, 415–422. DOI: 10.1007/s10450-007-9100-y.

Li G., Xiao P., Webley P.A., Zhang J., Singh R., 2009. Competition of CO_2/H_2O in adsorption based CO_2 capture. *Energy Procedia*, 1, 1123–1130. DOI: 10.1016/j.egypro.2009.01.148.

Li G., Xiao P., Zhang J., Webley P.A., 2014. The role of water on postcombustion CO_2 capture by vacuum swing adsorption: Bed layering and purge to feed ratio. *AIChE J.*, 60, 673–689. DOI: 10.1002/aic.14281.

Ling J., Ntiamoah A., Xiao P., Xu D., Webley P.A., Zhai Y., 2014. Overview of CO_2 capture from flue gas streams by vacuum pressure swing adsorption technology. *Austin Chem. Eng.*, 1 (2), 1009.

Marx D., Joss L., Hefti M., Pini R., Mazzotti M., 2013. The role of water in adsorption-based CO_2 capture systems. *Energy Procedia*, 37, 107–114. DOI: 10.1016/j.egypro.2013.05.090.

Petrus R., Warchoł J., Chutkowski M., 2006. Kinetyka sorpcji zanieczyszczeń ze środowiska wodnego na sorbentach naturalnych. *Prace Naukowe Instytutu Inżynierii Chemicznej PAN*, 7, 33–52.

Purdue M.J., Qiao Z., 2018. Molecular simulation study of wet flue gas adsorption on zeolite 13X. *Microporous Mesoporous Mater.*, 261, 181–197. DOI: 10.1016/j.micromeso.2017.10.059.

Qiu H., Lu L.V., Pan B.-C., Zhang Q.-J., Zhang W.-M., Zhang Q.-X., 2009. Critical review in adsorption kinetic models. *J. Zhejiang University – SCIENCE A*, 10, 716–724. DOI: 10.1631/jzus.A0820524.

Rashidi N.A., Yusup S., Loong L.H., 2013. Kinetic studies on carbon dioxide capture using activated carbon. *Chem. Eng. Trans.*, 35, 361–366. DOI: 10.3303/CET1335060.

Rege S.U., Yang R.T., Buzanowski M.A., 2000. Sorbents for air prepurification in air separation. *Chem. Eng. Sci.*, 55, 4827–4838. DOI: 10.1016/S0009-2509(00)00122-6.

Ryu Y.K., Lee S.J., Kim J.W., Lee C, 2001. Adsorption equilibrium and kinetics of H_2O on Zeolite 13X. *Korean J. Chem. Eng.*, 18, 525–530. DOI: 10.1007/BF0269830.

Sayılgan S.Ç., Mobedi M., Ülkü S., 2016. Effect of regeneration temperature on adsorption equilibria and mass diffusivity of zeolite 13X-water pair. *Microporous Mesoporous Mater.*, 224, 9–16. DOI: 10.1016/j.micromeso.2015.10.041.

Son K.N., Richardson T.J., Cmarik G.E., 2019. Equilibrium adsorption isotherms for H_2O on Zeolite 13X. *J. Chem. Eng. Data*, 64, 1063–1071. DOI: 10.1021/acs.jced.8b00961.

Tan K.L, Hameed B.H., 2017. Insight into the adsorption kinetics models for the removal of contaminants from aqueous solutions. *J. Taiwan Inst. Chem. Eng.*, 74, 25–48. DOI: 10.1016/j.jtice.2017.01.024.

Thomas W.J., Crittenden B., 1998. *Adsorption technology and design*. Butterworth-Heinemann.

Wang Y., LeVan M.D., 2009. Adsorption equilibrium of carbon dioxide and water vapor on zeolites 5A and 13X and silica gel: Pure components. *J. Chem. Eng. Data*, 54, 2839–2844. DOI: 10.1021/je800900a.

Wynnyk K.G., Hojjati B., Marriott R.A., 2018. High-pressure sour gas and water adsorption on zeolite 13X. *Ind. Eng. Chem. Res.*, 57, 15357–15365. DOI: 10.1021/acs.iecr.8b03317.

Zabielska K., Aleksandrzak T., Gabruś E., 2018. Adsorption equilibrium of carbon dioxide on zeolite 13X at high pressures. *Chem. Process Eng.*, 39, 309–321. DOI: 10.24425/122952.

Received 13 March 2020
Received in revised form 19 May 2020
Accepted 02 July 2020